

# Swift discovery of the orbital period of the HMXB IGR J015712–7259 in the Small Magellanic Cloud.

A. Segreto<sup>1</sup>, G. Cusumano<sup>1</sup>, V. La Parola<sup>1</sup>, A. D’Aì<sup>2</sup>, N. Masetti<sup>3</sup>, P. D’Avanzo<sup>4</sup>

<sup>1</sup> INAF – Istituto di Astrofisica Spaziale e Fisica Cosmica di Palermo, Via U. La Malfa 153, 90146 Palermo, Italy

<sup>2</sup> Dipartimento di Fisica e Chimica, Università di Palermo, via Archirafi 36, 90123, Palermo, Italy

<sup>3</sup> INAF - Istituto di Astrofisica Spaziale e Fisica Cosmica di Bologna, via Gobetti 101, 40129, Bologna, Italy

<sup>4</sup> INAF - Brera Astronomical Observatory, via Bianchi 46, 23807, Merate (LC), Italy

Preprint online version: November 12, 2017

## ABSTRACT

**Context.** In the last years the hard X-ray astronomy has made a significant step forward, thanks to the monitoring of the IBIS/ISGRI telescope on board the INTEGRAL satellite and of the Burst Alert Telescope (BAT) on board of the Swift observatory. This has provided a huge amount of novel information on many classes of sources.

**Aims.** We have been exploiting the BAT survey data to study the variability and the spectral properties of the new high mass X-ray binary sources detected by INTEGRAL. In this letter we investigate the properties of IGR J015712–7259.

**Methods.** We perform timing analysis on the 88-month BAT survey data and on the XRT pointed observations of this source. We also report on the broad-band 0.2–150 keV spectral analysis.

**Results.** We find evidence for a modulation of the hard-X-ray emission with period  $P_o = 35.6$  d. The significance of this modulation is 6.1 standard deviations. The broad band spectrum is modeled with an absorbed power law with photon index  $\Gamma \sim 0.4$  and a steepening in the BAT energy range modeled with a cutoff at an energy of  $\sim 13$  keV.

**Key words.** X-rays: general - : data analysis - stars: neutron - X-rays: individuals: IGR J015712–7259

## 1. Introduction

Since the first years of the last decade, astronomy has been having two profitable protagonists in the hard X-ray energy band: the IBIS/ISGRI telescope (Ubertini et al. 2003; Lebrun et al. 2003) on board the INTEGRAL satellite (Winkler et al. 2003) and the Burst Alert Telescope (BAT, Barthelmy et al. 2005) on board of the Swift observatory (Gehrels et al. 2004). IBIS/ISGRI has conducted a fruitful exploration of the Galactic Plane, revealing a large number of new X-ray sources: some of them are characterized by a strongly absorbed spectrum that made them elusive to previous soft X-ray monitoring; others show very bright transient episodes and they were revealed thanks to the continuous scan of the Galactic Plane. Many of these sources have been identified as high mass X-ray binaries (HMXBs), as inferred by the discovery of their optical counterparts (e.g., Filliatre & Chaty 2004; Reig et al. 2005; Masetti et al. 2006; Negueruela et al. 2006) and/or by the observation of long periodicities due to the occultation of the neutron star by the supergiant companion or to the enhancement of the neutron star accretion rate at periastron passage in an eccentric orbit. BAT is playing a momentous role in the study of many of these new INTEGRAL sources (e.g. Cusumano et al. 2010a; La Parola et al. 2010; D’Aì et al. 2011a,b). Thanks to a field of view two orders of magnitude larger than IBIS/ISGRI and to frequent changes of pointing direction, it efficiently records emission variability due to orbital eclipses or to the turn on of transient episodes.

IGR J015712–7259 is an X-ray binary discovered during the INTEGRAL scan of the Small Magellanic Cloud (SMC)

and of the Magellanic Bridge in December 2008. A Swift-XRT follow-up observation found the soft X-ray counterpart at RA= 01h 57m 16.4s, Dec=  $-72^\circ 58' 33''$  (J2000) with an uncertainty localization of  $3.8''$  (90% confidence level, Coe et al. 2008), and the USNO (Monet et al. 2003) star USNO-B1 0170-0064697, that lies within the XRT error box, was associated with IGR J015712–7259. The B and R magnitude of this star are 15.48 and 15.51, respectively (McBride et al. 2010). Timing analysis of the XRT and RXTE data revealed a periodicity of  $\sim 11.6$  s (Coe et al. 2008). A broad band spectral analysis that combines the XRT and ISGRI data showed a flat power law spectrum ( $\Gamma \sim 0.4$ ) with an exponential cutoff with a cutoff energy of  $\sim 8$  keV (McBride et al. 2010). This spectral shape is consistent with the spectrum typically shown by a HMXB.

This letter, that reports the results derived by the analysis of the soft and hard X-ray data collected by Swift on IGR J015712–7259, is organized as follows: section 2 describes the data reduction; section 3 reports on the timing analysis; in section 4 we describe the spectral analysis and in section 5 we briefly discuss our results.

## 2. Observations and data reduction

We have used the BATIMAGER code (developed for the analysis of coded mask telescopes data, see Segreto et al. 2010 for details) to analyze the data collected by Swift-BAT between November 2004 and March 2012 in survey mode. IGR J015712–7259 is detected in the 15–150 BAT all-sky map with a significance of  $\sim 7$  standard deviations in 88 months. The light curve of IGR J015712–7259 (Fig. 1) shows that the source is in a low intensity state in the first  $\sim 33$  months, rising to a higher state

Send offprint requests to: G. Cusumano, cusumano@ifc.inaf.it

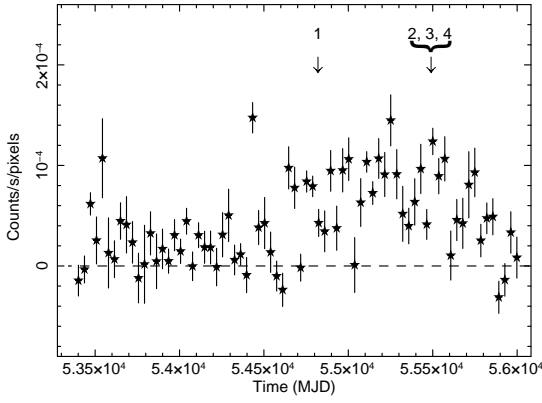


**Fig. 1.** IGR J015712–7259 BAT light curve the 15–45 keV energy range, with a bin length of 35 days. The epochs of the XRT observations are shown with vertical arrows.

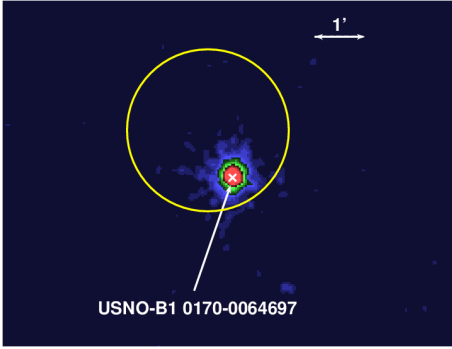


**Fig. 2.** 0.2–10 keV XRT image with superimposed the position of the optical counterpart, marked with a cross, and the BAT error circle of 1.61 arcmin (yellow circle).

throughout the following months. The significance of the source in this second interval rises to  $\sim 9$  standard deviation in the 15–150 keV band, and it is maximised to  $\sim 11$  standard deviations in the 15–45 keV energy band. Therefore, in order to study the timing and spectral properties of the source we have used the BAT data collected after MJD 54510. The light curve with the maximum resolution achievable with the BAT survey data was extracted in the 15–45 keV energy band.

The times were corrected to the Solar System barycentre (SSB) using the task `EARTH2SUN`<sup>1</sup> and the JPL DE-200 ephemeris (Standish 1982). The background subtracted spectrum averaged over the entire survey period was extracted in eight energy channels and analyzed using the BAT redistribution matrix available in the Swift calibration database<sup>2</sup>.

Swift-XRT observed IGR J015712–7259 four times, once in December 2008 (ObsID 00031313001) and three times in October 2010, for a total exposure time of  $\sim 12$  ksec. The details of each XRT observation are in Table 1. All the observations are in Photon Counting mode (Hill et al. 2004).

Data were processed with standard procedures, filtering and screening criteria (`XRTPIPELINE` v.0.12.4). Fig. 1 shows the 0.2–10 keV XRT image where the soft X-ray counterpart of IGR J015712–7259 is well within the BAT error circle (1.61 arcmin). We extracted the source events from a circular region (20 pixel radius, with 1 pixel corresponding to 2.36 arcsec)

**Table 1.** XRT observation log.

Obs #	Obs ID	$T_{start}$ (MJD)	$T_{elapsed}$ (s)	Exposure (s)	rate c/s	phase
1	00031313001	54820.3171	1985.7	1950.9	0.15	0.63
2	00041740001	55474.6958	23255.5	4613.9	0.02	0.03
3	00041740002	55488.2508	4461.2	4443.4	0.16	0.41
4	00041740003	55490.1957	29626.6	4214.4	0.26	0.46

**Notes.** The quoted phase refers to the profile in Figure 3c.

centered on the source centroid as calculated with `XRTCENTROID` (RA=01h 57m 15.9s, Dec= $-72^{\circ} 58' 29.9''$ , error radius 3.6"). The source events arrival times were corrected to the SSB using the task `BARYCORR`<sup>3</sup>. The background was extracted from an annular region with inner and outer radii 40 and 70 pixels, respectively. XRT ancillary response files were generated with `XRTMKARF`<sup>4</sup>. The source and background spectra of each observation were averaged to obtain a single spectrum, and the ancillary files were combined using `ADDARF`, weighting them by the exposure times of the relevant spectra. Both the summed spectrum and each single spectrum were rebinned with a minimum of 20 counts per energy channel, in order to allow the use of the  $\chi^2$  statistics. We used the spectral redistribution matrix `v013`. The spectral analysis was performed using `XSPEC` v.12.5. Errors are given at 90% confidence level, if not stated otherwise.

### 3. Timing analysis

The light curve of IGR J015712–7259 in the 15–45 keV energy range was investigated for the presence of periodic modulations. A timing folding analysis (Leahy et al. 1983) was applied to the barycentered arrival times. **This method consists in building the light curve profile at different trial periods by folding the photon arrival times in  $N$  phase bins. For each trial profile the  $\chi^2$  with respect to the average count rate is evaluated: a high  $\chi^2$  value will signal the presence of a periodic pulsation.** We searched in the 0.5–500 d period range with a step resolution of  $P^2/(N\Delta T)$ , where  $P$  is the trial period,  $N = 16$  is the number of folded profile phase bins and  $\Delta T$  ( $\sim 130$  Ms) is the data time span. The average rate in each phase bin was calculated weighting the light curve rates by the inverse square of the relevant statistical error. This procedure, adopted to deal with the large span in statistical errors, is justified by the fact that the data are characterized by a large range of **signal-to-noise ratio** because BAT monitors the source over a wide range of off-axis directions. Figure 3a shows the resulting periodogram. We find several features emerging over the  $\chi^2$  average trend. The feature at the lowest period is at  $P_0 = 35.6 \pm 0.5$  d ( $\chi^2 \sim 132$ ) where the period and its error are evaluated as the position of the centroid and the standard deviation obtained from a Gaussian fit of the periodogram feature. The features at higher  $P$  result to be multiples of  $P_0$ .

The average  $\chi^2$  in the periodogram increases monotonically with the trial period deviating from what is expected for a white noise signal, where the  $\chi^2$  is expected to have an average value of  $(N - 1)$ . As a consequence, we cannot apply the  $\chi^2$  statistics to evaluate the significance of the feature at  $P_0$  and an ad hoc procedure has to be used. The following steps summarize what we have done to estimate the significance of the feature:

<sup>1</sup> <http://heasarc.gsfc.nasa.gov/ftools/fhelp/earth2sun.txt>

<sup>2</sup> <http://swift.gsfc.nasa.gov/docs/heasarc/caldb/swift/>

<sup>3</sup> <http://heasarc.gsfc.nasa.gov/ftools/caldb/help/barycorr.html>

<sup>4</sup> <http://heasarc.gsfc.nasa.gov/ftools/caldb/help/xrtmkarf.html>

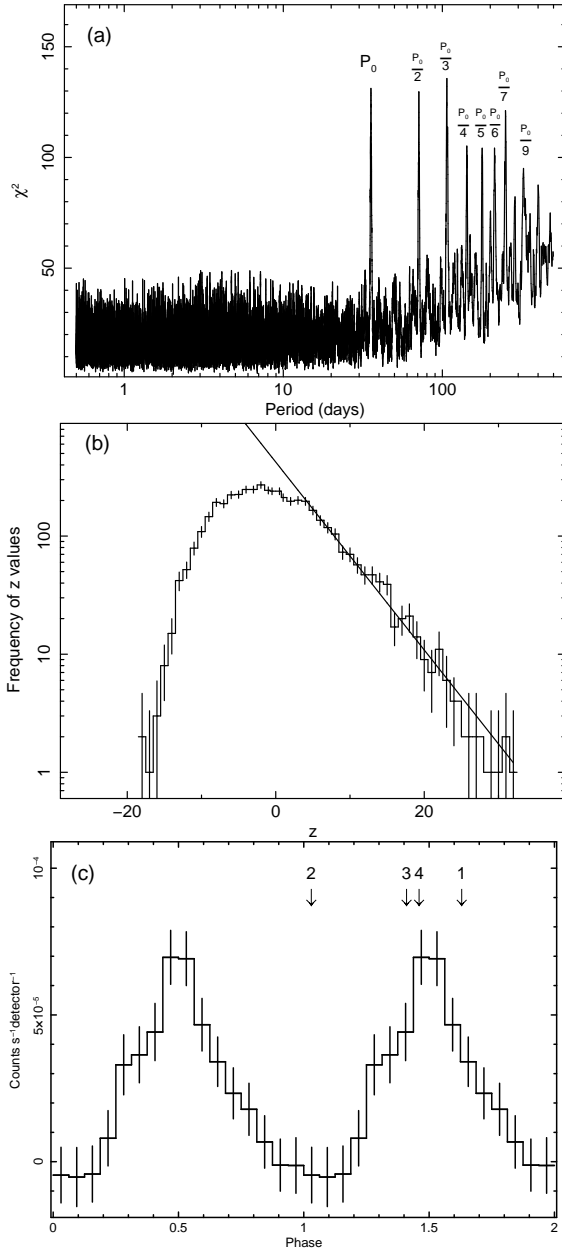


**Fig. 3.** (a): Periodogram of *Swift*-BAT (15–45 keV) data for IGR J015712–7259. (b): Histogram of the  $z$  ( $\chi^2 - F_{\chi^2}$ ) distribution. The continuous line represents the best fit exponential model for  $z > 20$ . (c): *Swift*-BAT light curve folded at a period  $P_0 = 35.6$  d, with 16 phase bins. Two orbital cycles are shown for clarity. The phase relevant to the epoch of each XRT observation is shown with a vertical arrow.

(1) we modeled the  $\chi^2$  distribution with a 2nd order polynomial to derive the average trend  $F_{\chi^2}(P)$  of the  $\chi^2$  versus  $P$ .

(2)  $F_{\chi^2}$  was then subtracted from the  $\chi^2$  distribution to obtain a flattened periodogram (hereafter,  $z$ ). This allows to evaluate the significance of the feature with respect to the average noise level of the periodogram. The value of  $z$  corresponding to  $P_0$  is  $\sim 110$ .

(3) We built the histogram of the  $z$  distribution (Figure 3b) from  $P=15$  d to  $P=55$  d (where the periodogram is characterized by a noise level quite consistent with the noise level  $P_0$ ) at excluding the interval around  $P_0$ .

(4) We modeled the positive tail ( $z > 5$ ) of the histogram with an exponential function.

(5) We evaluated the area ( $\Sigma$ ) of the  $z$  histogram summing the contribution of each single bin from its left boundary up to

$z=5$  and integrating the best-fit exponential function beyond  $z=5$  up to infinity.

(6) We evaluated the integral of the best-fit exponential function between  $z=110$  and infinity and normalized it dividing by  $\Sigma$ .

The result ( $\sim 8.5 \times 10^{-10}$ ) is the probability of chance occurrence to find a  $z$  value  $\geq 110$  (or  $\chi^2 \geq 132$ ) and it corresponds to a significance for the  $P_0$  feature of  $\sim 6.1$  standard deviations in Gaussian statistics.

In Fig. 3 (c) we show the BAT light curve folded at  $P_0$  with a  $T_{\text{epoch}} = 55224.8086$  MJD. The profile is characterized by a single symmetric peak with a minimum consistent with null intensity, whose centroid, evaluated by fitting the data around the dip with a Gaussian function, is at phase  $1.01 \pm 0.02$  corresponding to MJD ( $55225.2 \pm 0.7$ )  $\pm nP_0$ . The peak is at phase  $1.50 \pm 0.02$ , corresponding to MJD  $55242.6 \pm 0.7 \pm nP_0$ .

The phase corresponding to the epochs of the XRT observations and referred to the folded BAT light curve are represented in Figure 3c by vertical arrows. The rates averaged over each observation (column 6 in Table 1) show a variability in good agreement with the BAT rate profile.

In order to search for the pulsed modulation at  $\sim 11.6$  s we have applied the folding analysis to XRT pointings 1 and 4 in Table 1 (pointings 2 and 3 have a low statistic content, with  $\sim 70$  counts each). The periodogram derived from observation 1 shows a feature at  $P_s = 11.58 \pm 0.01$  s ( $\chi^2 = 36.6$ , 7 d.o.f.), where the error is  $P_s^2/(N\Delta T)$ , with  $N=8$ , confirming the result reported by Coe et al. (2008). The probability of chance occurrence for a feature with such a  $\chi^2$  value at 11.6 s is  $\sim 8 \times 10^{-6}$ , corresponding to a significance of  $\sim 4.5$  standard deviations in Gaussian statistics. The periodogram of observation 4 does not show any significant feature. We also performed a folding analysis on each of the five snapshots of observation 4, without finding any significant feature either in each single snapshot periodogram or in the periodogram produced by their sum.

#### 4. Spectral analysis and results

The broad band spectral analysis puts together XRT data of different epochs and BAT data accumulated over the 88-month of monitoring. We therefore performed a preliminary analysis to verify that no significant spectral variability affects the 4 XRT observations and during the BAT monitoring. The background subtracted spectra of each single XRT observation were fitted simultaneously with an absorbed power law with the photon index and absorbing column density forced to have the same value for the 4 datasets. This model, yielding a best fit photon index of  $0.99 \pm 0.12$  and  $N_{\text{H}}$  of  $(1.5 \pm 0.5) \times 10^{21}$  cm $^{-2}$ , produced residuals with a similar trend for all the datasets. Different BAT spectra were also produced selecting the data in different time intervals (MJD intervals 53383.478–54593.061, 54593.061–55233.428, and 55233.428–56016.101; see Figure 1) and in three different phase intervals (0.94–1.31, 0.31–0.44 plus 0.69–0.81, and 0.44–0.69, see Figure 3). These spectra were fitted with a power law model and, as above, we forced the photon index to assume the same value for all the spectra leaving the normalization free to vary. The residuals between best fit model and data showed a similar trend for all the datasets. The best fit photon index is  $2.0 \pm 0.2$ .

The broad band spectral analysis was then performed coupling the 15–150 keV BAT spectrum extracted from the data collected after MJD 54510 and the XRT spectrum obtained by adding the individual XRT spectra (see Sect. 2). A multiplicative factor that disengages the normalization parameter of the model for the two datasets was introduced in the fit to take into

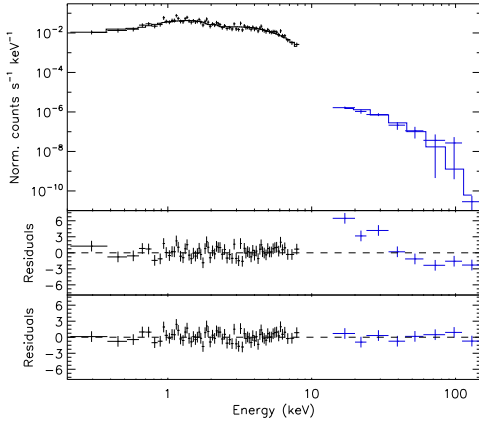


**Fig. 4.** IGR J015712–7259 broad band spectrum. **Top panel:** XRT and BAT data and best fit `phabs*cutoffpl` model. **Central panel:** Residuals in unit of standard deviations for the `phabs*powerlaw` model. **Bottom panel:** Residuals in unit of standard deviations for the `phabs*cutoffpl` model.

**Table 2.** Best fit spectral parameters.

Parameter	Cutoff pl	Units
$N_{\text{H}}$	$< 5 \times 10^{20}$	$\text{cm}^{-2}$
$\Gamma$	$0.4^{+0.1}_{-0.1}$	
$E_{\text{cut}}$	$13^{+4.0}_{-3.0}$	keV
$N$	$5.2^{+0.6}_{-0.4} \times 10^{-4}$	ph / (keV $\text{cm}^2 \text{s}$ ) at 1 keV
$C_{\text{BAT}}$	$0.4^{+0.2}_{-0.1}$	
F (0.2–10 keV)	$1.26^{+0.11}_{-0.12} \times 10^{-11}$	$\text{erg cm}^{-2} \text{s}^{-1}$
F (15–150 keV)	$9.1^{+1.3}_{-2.4} \times 10^{-12}$	$\text{erg cm}^{-2} \text{s}^{-1}$
$\chi^2$	70.1 (75 dof)	

**Notes.**  $C_{\text{BAT}}$  is the constant factor to be multiplied to the model in the BAT energy range in order to match the BAT data. We report unabsorbed fluxes for the characteristic XRT (0.2–10 keV) and BAT (10–150 keV) energy bands.

account both the intercalibration uncertainty between XRT and BAT and the non simultaneity of the data. We started fitting the data with an absorbed power law model `phabs*(powerlaw)`. This model yields an unacceptable  $\chi^2=149.7$ , with 76 degrees of freedom [dof] and is not able to describe the BAT data, as shown in Figure 4, (middle panel). The steepening in the BAT energy range (see figure 4) suggesting the presence of a cut-off. Indeed, the spectrum turned out to be much better described adopting the model `phabs*cutoffpl` (see table 2) with a photon index  $\Gamma$  of  $\sim 0.4$  and an folding energy of  $\sim 13$  keV, resulting in a  $\chi^2 = 70.1$ , for 75 dof. The hydrogen column density is lower than  $5 \times 10^{20} \text{cm}^{-2}$ . Figure 4 shows data and best fit model (top panel) and residuals (bottom panel) for the cutoff powerlaw model.

## 5. Conclusions

IGR J015712–7259, discovered by INTEGRAL in the SMC, is a HXMB with an X-ray emission modulated by a spin period of 11.6 s (Coe et al. 2008). The timing analysis of the BAT survey data has allowed to add a new piece of information on this binary system, with the discovery of a long term periodic modulation in its hard X-ray emission at  $P_o = 35.6 \text{ d}$ . The significance of this result is  $\sim 6.1$  standard deviations in Gaussian statistics. We interpret this modulation as the orbital period of the binary system. Its knowledge, together with the spin period measurement allows us to locate the source on the Corbet diagram (Corbet 1986), where its position is consistent with the Be X-ray binaries region (Figure 5). On the other hand, the BAT light curve

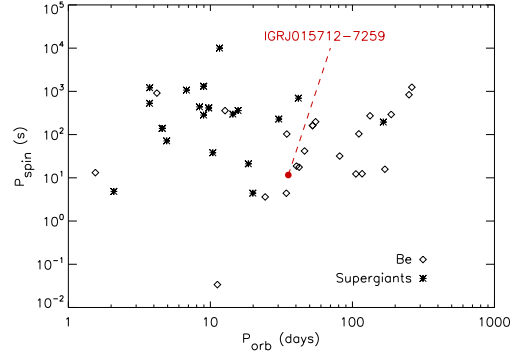


**Fig. 5.** The Corbet diagram plots the spin period versus the orbital period for HMXBs. Diamond and star points represent the Be and supergiant systems, respectively. The red filled circle marks the position of IGR J015712–7259.

folded at  $P_o$  shows a triangular symmetric peak with a minimum consistent with zero intensity suggesting that accretion happens for most of the orbit. The minimum could be related to the occultation of the neutron star by the companion star. This behavior is not typical for HXRB with a Be companion, that usually are observed through short-lived enhancements of their emission caused by accretion episodes driven either by disk instabilities or to the periastron passage in a highly eccentric orbit.

The BAT long-term light curve (Figure 1) shows that this source has enhanced its hard X-ray activity since early 2009, after showing a modest intensity level in the first three years of the survey monitoring. This behavior prevented the source from being reported in the first Palermo BAT catalogues (Cusumano et al. 2010b,c), while it is listed with a significance of  $\sim 10$  standard deviations in the latest issue of the catalogue<sup>5</sup> (that covers 66 months of survey). The INTEGRAL detection reported by Coe et al. (2008) is located in time during the early stages of enhanced emission.

The broad-band (0.2–150 keV) spectral analysis of IGR J015712–7259 was performed combining all the available Swift-XRT observations and the BAT spectrum extracted from the data collected after MJD 54510 when the source is observed to be in a high intensity state. The data are well described by a flat ( $\Gamma \simeq 0.4$ ) powerlaw with a cut-off at  $\sim 13$  keV. This spectral shape is commonly observed among HMXBs. The best fit parameters are in agreement with the analysis reported by McBride et al. (2010) based on the December 2008 XRT observation and on the ISGRI data.

The results reported above need to be integrated with optical observations aimed at the identification of the spectral type of the companion star. This will allow to ascertain the class of this binary system and to set more constraints on its orbital characteristics.

*Acknowledgements.* This work has been supported by ASI grant I/011/07/0.

## References

- Barthelmy, S. D., et al. 2005, *Space Science Reviews*, 120, 143  
Coe M. J., McBride V. A., Bird A. J., Corbet R.H.D., et al., 2008, *ATEL* 1882  
Corbet, R. H. D. 1986, *MNRAS*, 220, 1047  
Cusumano, G., La Parola, V., Romano, P., et al. 2010, *MNRAS*, 406, L16

<sup>5</sup> <http://bat.ifc.inaf.it>

- Cusumano, G., La Parola, V., Segreto, A., et al. 2010, *A&A*, 524, A64  
Cusumano, G., La Parola, V., Segreto, A., et al. 2010, *A&A*, 510, A48  
D’Ai, A., Cusumano, G., La Parola, V., et al. 2011, *A&A*, 532, A73  
D’Ai, A., La Parola, V., Cusumano, G., et al. 2011, *A&A*, 529, A30  
Filliatre, P., & Chaty, S. 2004, *ApJ*, 616, 469  
Gehrels, N., et al. 2004, *ApJ*, 611, 1005  
Hill, J. E., Burrows, D. N., Nousek, J. A., et al. 2004, *Proc. SPIE*, 5165, 217  
La Parola, V., Cusumano, G., Romano, P., et al. 2010, *MNRAS*, 405, L66  
Lebrun, F., Leray, J. P., Lavocat, P., et al. 2003, *A&A*, 411, L141  
Leahy, D. A., Darbro, W., Elsner, R. F., et al. 1983, *ApJ*, 266, 160  
Masetti, N., Morelli, L., Palazzi, E., et al. 2006, *A&A*, 459, 21  
McBride, V. A., Bird, A. J., Coe, M. J., et al. 2010, *MNRAS*, 403, 709  
Monet, D. G., Levine, S. E., Canzian, B., et al. 2003, *AJ*, 125, 984  
Negueruela, I., Smith, D. M., Reig, P., Chaty, S., & Torrejón, J. M. 2006, *The X-ray Universe 2005*, ed. A. Wilson, *ESA Special Publication*, 604, 165  
Reig, P., Negueruela, I., Papamastorakis, G., Manousakis, A., & Kougentakis, T. 2005, *A&A*, 440, 637  
Segreto, A., Cusumano, G., Ferrigno, C., La Parola, V., Mangano, V., Mineo, T., & Romano, P. 2010, *A&A*, 510, A47  
Standish, E. M., Jr. 1982, *A&A*, 114, 297  
Ubertini, P., Lebrun, F., Di Cocco, G., et al. 2003, *A&A*, 411, L131  
Winkler, C., Courvoisier, T. J.-L., Di Cocco, G., et al. 2003, *A&A*, 411, L1